To be published in OSA Continuum:

Title: Noise amplification in all-normal dispersion fiber supercontinuum generation and its impact in ultrafast photonics applications

Authors: Benoît Sierro,Alexander Heidt

Accepted: 27 July 20

Posted 27 July 20

DOI: https://doi.org/10.1364/OSAC.397603

Noise amplification in all-normal dispersion fiber supercontinuum generation and its impact in ultrafast photonics applications

BENOÎT SIERRO* AND ALEXANDER M. HEIDT

Institute of Applied Physics, University of Bern, Sidlerstrasse 5, 3012 Bern, Switzerland
sierro.benoit@iap.unibe.ch

Abstract: Highly coherent and low-noise supercontinuum (SC) sources based on nonlinear spectral broadening of femtosecond pulses in all-normal dispersion (ANDi) fibers are attractive for many applications in ultrafast photonics. By simulating a real nonlinear pulse compression experiment, we numerically investigate the impact of shot noise and technical pump laser fluctuations on the quality and stability of single-cycle pulse generation and other multi-shot experiments based on the manipulation of the SC spectral phase. We find that for pump pulse durations of less than 600 fs, input relative intensity noise <1%, and correctly chosen fiber lengths, the initial fluctuations of the pump laser are at most amplified by a factor of three. We also show that the usual strong correlation between SC coherence and quality of the compressed pulses collapses in the presence of technical noise, and that in this situation the coherence is not a useful figure of merit to quantify pulse quality, noise amplification, or decoherence due to incoherent nonlinear dynamics. Our results highlight the very limited impact of technical pump laser noise on ANDi SC generation and are of practical relevance for many ultrafast photonics applications that require high-quality, low-noise SC sources.

1. Introduction

The nonlinear spectral broadening of femtosecond pulses in all-normal dispersion (ANDi) fibers has emerged as an attractive way of realizing low-noise, highly coherent, and octave-spanning supercontinuum (SC) sources [1]. ANDi SC are particularly attractive for ultrafast photonics applications since their smooth and stable spectral phase can easily be compensated using static or active compression devices, resulting in the generation of high quality, Fourier-limited few- or even single-cycle pulses [2–5]. When considering nonlinear pulse compression based on solid core optical fibers, the ANDi fiber design has enabled (i) the shortest pulse duration (3.7 fs, 1.3 cycles at 800 nm) [6], (ii) the highest pulse quality (20 dB pre- and post-pulse suppression) [6], and (iii) the highest compression ratio to the sub-two cycle regime (28×, 180 fs to 6.4 fs, 1.8 cycles at 1040 nm) [7]. Although conventional SC sources, which make use of femtosecond pulses launched into the anomalous dispersion regime of a fiber, can generate broader spectral bandwidths and should therefore give rise to even shorter pulses, in practice the complex fine structure of the spectral phase and its noise sensitivity have prevented their compression to the sub-two cycle regime, even when maximising the coherence using very short pump pulses and very short fiber lengths [8–10]. Consequently, ANDi SC sources are the preferred choice for ultrafast photonics and have found applications, e.g. in nonlinear bio-photonic imaging, ultrafast spectroscopy, coherent X-ray generation, attoscience, and low-noise ultrafast fiber laser development, with spectral coverage extending from UV to mid-IR wavelengths. [11–23].

The noise properties of the SC are of particular importance for ultrafast photonics applications since efficient temporal compression or phase-shaping is only possible when the spectral phase remains stable from shot to shot, which is usually associated with a high degree of temporal coherence [9]. Potential fluctuations of the SC translate to intensity noise, pulse duration

noise, or timing jitter of the compressed pulse train, which affect the sensitivity, resolution, or synchronisation of ultrafast experiments [8, 24]. While the impact of quantum and various technical noise sources on the stability of conventional SC has been studied extensively already over a decade ago [25–27], the noise limitations of ANDi SC have only recently started to be investigated. Numerical studies of the fundamental coherence limits have found that the low-noise, high coherence properties of octave-spanning ANDi SC are maintained even for very long pump pulses up to about 1 ps duration if these pump pulses are shot-noise limited [28]. While polarisation noise effects can drastically reduce the stability of ANDi SC, this can be completely avoided by employing only polarisation-maintaining fibers [17, 29–31]. These results suggest that ANDi SC should be perfectly suitable for ultrafast experiments, including nonlinear pulse compression to the single-cycle regime, for pump pulse durations up to about 1 ps. This is quite remarkable when compared to their conventional SC counterparts, which start to exhibit significant quantum noise amplification and associated instabilities already for 100 fs pulse durations and short fiber lengths, even when considering shot noise limited input [25, 27, 32].

The impact of technical noise on ANDi SC generation, such as relative intensity noise (RIN) of the pump pulses at levels higher than the shot-noise limit, has been subject of several recent numerical and experimental studies [33–37], with somewhat contradictory results. While it was found that the ANDi SC generation dynamics do not significantly amplify technical noise and that the RIN of the SC in the central part of the spectrum can actually be lower than the RIN of the mode-locked pump laser itself, it was observed that technical noise drastically affects the SC coherence, which starts degrading already at pump pulse durations of 50 - 100 fs if a weak pump laser RIN is taken into account [35]. This result could have serious consequences for the applicability of ANDi SC in nonlinear pulse compression and ultrafast photonics in general, since reduced SC coherence is usually associated with poor compressed pulse quality and significant intensity, pulse duration, and timing jitters [9].

In this paper we consider this problem in more detail, following the numerical procedure outlined in Ref. [9] for the simulation of a realistic nonlinear pulse compression experiment and studying in particular the compressed pulse characteristics in the presence of both quantum and technical noise sources. In this way, we are able to compare the noise characteristics of the pump pulses and the compressed pulses directly in the time domain and determine whether different types of technical noise experience suppression, amplification, or remain constant during the ANDi SC generation process. We focus in particular on the quality of the compressed single-cycle pulses that can be expected in a real experiment as a function of input pulse duration and technical noise level, and study the relationship between pulse quality and SC coherence in the presence of technical noise.

We use nonlinear pulse compression as our test scenario as it is straightforward to implement in a numerical simulation. However, we emphasize that our results apply to a wide range of different ultrafast ANDi SC applications, which often involve the manipulation of the SC spectral phase in multi-shot experiments and are therefore subject to the very similar noise limitations.

2. Numerical model

This study is based on a numerical solution of the single-mode generalized nonlinear Schrödinger equation (GNLSE) in the frequency domain [38]. Propagation in the forward direction in one polarization axis is assumed. The model includes higher-order dispersion up to 10th order as well as all relevant nonlinear effects, i.e. instantaneous Kerr-type and delayed Raman response, self-steepening, and shock formation terms. The solver uses a 4th order Runge-Kutta method in the Interaction Picture (RK4IP) [39], and runs both efficiently and accurately due to an adaptive step size algorithm based on photon number conservation [40]. The relative threshold for step-to-step numerical errors has been set to 10^{-11} for every simulation and we use 2^{15} frequency bins with a temporal resolution of 1.13 fs. Since we expect compressed pulses with smooth

envelopes of around 5 fs duration, we use spline interpolation to better measure their properties.

We base our calculations on the model fiber with ANDi profile optimized for pumping at wavelengths around 1 µm that was previously used for studying the fundamental coherence limits of SC generation in normal dispersion fibers [28]. It is a hexagonal lattice silica PCF with design parameters pitch $\Lambda = 1.5\,\mu\text{m}$ and relative hole size $\phi/\Lambda = 0.37$, whose dispersion profile with maximum of $D = -19$ ps/(nm km) at 1014 nm was calculated using a simple semi-analytical approach [41, 42]. The Taylor series expansion coefficients at our chosen pump wavelength of 1050 nm are given in Table 1. For simplicity, we assume a constant nonlinear parameter $\gamma = 0.018\,\text{W}^{-1}\,\text{m}^{-1}$ that corresponds to an effective mode field area $A_{\text{eff}} = 8.6\,\mu\text{m}^2$, neglect fiber loss, and model the delayed Raman response function as in [43]. Fibers with very similar dispersion profiles are available commercially, and were also used in recent numerical and experimental studies on the impact of polarization-dependent noise and technical pump laser noise on the coherence and noise properties of ANDi SC [29, 35]. Hence, our results can be related directly to previous literature and subjected to future experimental validation.

$\beta_2 =$	$1.001\,190 \cdot 10^{1}$ ps^2/km	$\beta_7 =$	$1.696\,410 \cdot 10^{-11}$ ps^7/km
$\beta_3 =$	$-2.131\,124 \cdot 10^{-2}$ ps^3/km	$\beta_8 =$	$-9.261\,236 \cdot 10^{-14}$ ps^8/km
$\beta_4 =$	$3.286\,793 \cdot 10^{-4}$ ps^4/km	$\beta_9 =$	$2.149\,311 \cdot 10^{-16}$ ps^9/km
$\beta_5 =$	$-1.290\,523 \cdot 10^{-6}$ ps^5/km	$\beta_{10} =$	$-2.028\,394 \cdot 10^{-19}$ ps^{10}/km
$\beta_6 =$	$1.047\,255 \cdot 10^{-9}$ ps^6/km		

Table 1. Taylor series expansion coefficients at 1050 nm for the dispersion profile of the PCF. $\Lambda = 1.5\,\mu\text{m}$ (pitch) and $\phi = 0.56\,\mu\text{m}$ (hole diameter).

In this study we consider a pump laser exhibiting two different kinds of noise: (i) quantum (shot) noise, and (ii) technical amplitude noise anti-correlated with pulse duration jitter. Both can be modelled using modifications of an ideal Gaussian pump field. Quantum shot noise is represented as one photon with random phase added into each frequency bin, while technical noise is modelled as shot-to-shot field amplitude variations. In order to facilitate the comparison of our results with previous literature, we follow the definition of technical noise recently given in Ref. [35] based on measurements of a real pump laser. For a given input peak power P_0, the peak field amplitude $\sqrt{P_0}$ of each pump pulse is multiplied by a number $1 + \Psi$, where Ψ is randomly picked from a normal distribution with mean 0 and standard deviation δ_A equal to the noise parameter of the pump laser given in percent. The temporal width is considered to be anti-correlated with the amplitude [35]. The input spectral amplitude $\tilde{A}_0$ is thus:

$$\tilde{A}_0(\omega) = \mathcal{F}\left\{(1+\Psi)\sqrt{P_0}\exp\left[-\left(\frac{t}{(1-0.8\Psi)T_0}\right)^2\right]\right\} + \delta_N(\omega) \tag{1}$$

where ω is angular frequency, $\mathcal{F}$ denotes the Fourier transform, t is the time in the co-moving frame of reference, T_0 relates to the full width at half maximum $T_{0,\text{FWHM}} = \sqrt{2\ln 2}T_0$, and $\delta_N(\omega) = \sqrt{h\omega/\text{d}\omega}\exp(-i\Phi(\omega))$ is the quantum noise in the frequency domain, with Planck's constant h, frequency bin size $\text{d}\omega$ and random phase $\Phi(\omega)$ sampled in the interval $[0; 2\pi]$. Note that in this definition and for small δ_A, the experimentally accessible RIN $\delta_I = (1+\delta_A)^2 - 1 \approx 2\delta_A$. Although the effects of technical noise on its own can be assessed using only a few simulations [25], evaluating both quantum and technical noise sources combined requires ensemble averages in order to compute coherence properties and statistical noise values. Hence, we repeat each

simulation multiple times using different randomly generated noise seeds, and found an ensemble size of 20 independent simulations sufficient to achieve convergence of the statistical noise values. No noticeable change was observed for larger ensemble sizes, but it should be noted that recovering the distribution of δ_A programmed into the simulation is not guaranteed. For this reason, we determine the real RIN and pulse duration noise value of each generated ensemble and give these values throughout the manuscript, unless otherwise stated.

3. Simulating quality and noise properties of compressed pulses

We focus our numerical investigation on assessing the quality and noise properties of the compressed pulse train that could be expected in a real multi-shot experiment. Physical phase compensation devices, e.g. spatial light modulators, are unable to adaptively follow noise-induced shot-to-shot fluctuations of the spectral phase, but instead can only be set to compensate the mean spectral phase of the pulse train. To simulate the compression process, at the exit of the fiber we write the spectral envelope as an amplitude $|\tilde{A}|$ and a phase Φ

$$\tilde{A}(\omega) = |\tilde{A}(\omega)|e^{i\Phi(\omega)}, \tag{2}$$

compute a mean phase across 20 simulations, and find an individual compressed field envelope A_c

$$A_c(t) = \mathcal{F}^{-1}\left\{|\tilde{A}(\omega)|e^{i(\Phi(\omega)-\langle\Phi(\omega)\rangle)}\right\}, \tag{3}$$

where $\langle\Phi(\omega)\rangle$ denotes the ensemble average over a set of 20 simulations. Any phase fluctuation results in a different residual spectral phase of each pulse leading to intensity, pulse duration, and timing jitters of the compressed pulse train, and causing shot-to-shot variations of the pulse shape.

The quality of the average compressed pulse available for a multi-shot ultrafast experiment strongly depends on the magnitude and correlations of these shot-to-shot fluctuations. The fraction of the total pulse energy contained in the central lobe of the average compressed pulse is often used as a figure of merit for the pulse quality [9]. However, this figure does not only depend on noise-induced fluctuations, but also on the shape of the spectral envelope that continuously evolves during SC generation. In order to focus on the impact of noise on the pulse quality, it is useful to define a normalized figure of merit eliminating the dependence on the spectral envelope. In ultrafast optics the Fourier-limited pulse $A_{\mathrm{fl}}(t)$ of a given laser source is often estimated by taking the inverse Fourier transform of the spectral intensity measured with a slow spectrometer assuming a flat spectral phase, i.e.

$$A_{\mathrm{fl}}(t) = \mathcal{F}^{-1}\left\{\sqrt{\langle|\tilde{A}(\omega)|^2\rangle}\right\}. \tag{4}$$

Therefore, we define the normalized pulse quality factor F_{Q} as the ratio between the fraction of total energy in the central lobe of the mean compressed pulse and the energy fraction in the central lobe of the ideal, Fourier-limited pulse,

$$F_{\mathrm{Q}} = \frac{\eta\left(\langle A_c(t)\rangle\right)}{\eta\left(A_{\mathrm{fl}}(t)\right)}, \quad \eta\left(A(t)\right) = \frac{\int_{t_{\mathrm{central}}}|A(t)|^2\mathrm{d}t}{\int_{-\infty}^{\infty}|A(t)|^2\mathrm{d}t}, \tag{5}$$

where t_{central} is the duration of the central lobe. $F_Q = 1$ in the absence of noise, while its value decreases with increasing fluctuations of the pulse train.

Additionally, by compiling every one of the 190 possible pairs of spectra $[\tilde{A}_1, \tilde{A}_2]$, we also compute the mean coherence $\langle|g_{12}|\rangle$ in the usual way [27],

$$|g_{12}(\omega)| = \left|\frac{\langle\tilde{A}_1^*(\omega)\tilde{A}_2(\omega)\rangle}{\sqrt{\langle|\tilde{A}_1(\omega)|^2\rangle\langle|\tilde{A}_2(\omega)|^2\rangle}}\right|, \tag{6}$$

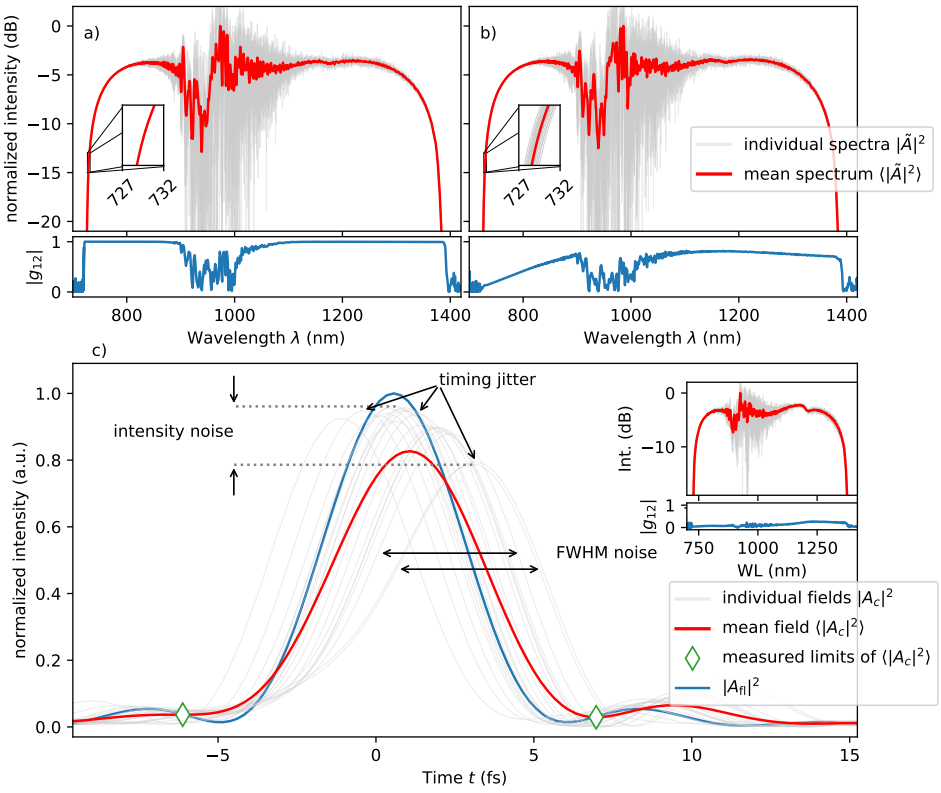

Fig. 1. Illustration of the considered noise effects. Individual spectra, mean spectrum and coherence of an ensemble of 20 simulations of 100 kW, 600 fs pulses after 1 m of propagation considering (a) only quantum noise ($\delta_A = 0$), and (b) additional 0.5% intensity noise (0.19% pulse duration noise). (c) Temporal profiles of 100 kW, 800 fs initial pulses with 0.9% intensity noise (0.38% pulse duration noise) compressed after $3.2L_{\mathrm{WB}} = 65$ cm of propagation. The inset shows corresponding spectra and coherence.

$$\langle|g_{12}|\rangle = \frac{\int_0^\infty |g_{12}(\omega)| \cdot \langle|\tilde{A}(\omega)|^2\rangle \mathrm{d}\omega}{\int_0^\infty \langle|\tilde{A}(\omega)|^2\rangle \mathrm{d}\omega}. \tag{7}$$

$\langle|g_{12}|\rangle$ and F_Q are used together with the standard deviations of pulse duration, peak intensity and timing jitters as metrics to assess the pulse quality.

4. Results

Fig. 1 (a) and (b) illustrate the impact of quantum and technical noise on the generated SC spectra and their coherence properties. An input pulse with duration $T_{0,\mathrm{FWHM}} = 600$ fs and peak power $P_0 = 100$ kW is considered, propagated over 1 m fiber length (the same P_0 is used throughout this work). In (a), only the quantum noise term δ_N is added to the input pulse, while in (b) both quantum noise and additional technical noise with 0.5% RIN, corresponding to 0.19% relative pulse duration jitter, are considered.

Clearly, the effects of the two noise terms are qualitatively very different. Quantum noise is subject to nonlinear amplification by stimulated Raman scattering (SRS) and parametric

four-wave mixing (FWM), leading to the strong fluctuations and the coherence collapse in the 900 nm to 1100 nm range in both plots, as described in detail in Ref. [28]. Similar to amplified quantum noise in conventional SC, this leads to a white noise RIN exhibiting very high frequency components which substantially exceed the reciprocal pulse duration, i.e. in the frequency range > 10 THz [26]. In contrast, the action of technical noise is much less dramatic and mainly results in minimal shot-to-shot variation of the spectral bandwidth, as highlighted in the magnified section of the short-wavelength edge between 727 - 732 nm in Fig. 1 (b). These fluctuations are not caused by incoherent nonlinear dynamics, but simply arise from the sensitivity of the GNLSE to the input pulse parameters. For example, the spectral bandwidth of ANDi SC is approximately proportional to $\sqrt{P_0}$ [1, 28]. Therefore, fluctuations of the peak intensity are translated to shot-to-shot spectral bandwidth variations, dampened by the square root factor. Consequently, for a train of SC pulses with repetition rate f_{rep} technical noise only occurs at frequencies lower than the Nyquist frequency, $f_{\mathrm{rep}}/2$, i.e. typically in the Hz - MHz range. Hence, quantum and technical noise are usually well separable in the frequency domain. Nevertheless, the coherence function $|g_{12}|$ strongly reacts to these low-frequency technical fluctuations and decreases substantially, especially on the short-wavelength side of the spectrum.

The effect of these spectral fluctuations on the compressed pulses is shown in Fig. 1 (c). We chose a quite noisy SC generated by an input pulse of 800 fs duration with 0.9% intensity noise propagated over an excessive fiber length of 3.2 times the optical wave breaking length (L_{WB}), i.e. 65 cm, which leads to a complete collapse of the coherence function, as shown in the inset. We then compress the simulated ensemble according to Eq. (3), compute the mean pulse $\langle A_c(t)\rangle$ that would be measured by a multi-shot pulse characterization device, and compare it to the Fourier-limited pulse computed with Eq. (4). We can clearly distinguish three different kinds of fluctuations : (i) timing jitter, (ii) pulse duration (FWHM) noise, and (iii) peak intensity noise. The diamond shapes on the plot indicate the limits of the central lobe of the mean pulse, which are used in the computation of the quality factor, Eq. (5), to determine the fraction of energy contained in the central lobe.

Using the particular example shown in Fig. 1 (c) we highlight some general noise properties of the compressed pulses observed in our simulations. Firstly, it is evident that the timing jitter is the dominant noise source, reaching the same order of magnitude as the compressed FWHM pulse duration. This jitter is introduced by uncompensated linear phase components of the individual pulses in the ensemble. In comparison, intensity and pulse duration noise play a secondary role. Secondly, the pulse shape is very well preserved from shot to shot, and the fluctuations occur in a quite symmetrical fashion around the mean. As a consequence, and although the coherence has completely collapsed, the mean compressed pulse that would be measured by a multi-shot characterisation method retains a very good quality, reflected in a quality factor $F_{\mathrm{Q}} = 98\%$, albeit with a 17 % drop in peak power and an increase in pulse duration from 4.9 fs to 5.6 fs compared to the Fourier limit. This is a first indication that the close correlation of average coherence and compressed pulse quality reported for anomalous-dispersion SC is violated for ANDi SC in the presence of technical noise, and that a more detailed analysis is required to judge the applicability of compressed ANDi SC pulse for a particular ultrafast application.

Interestingly, previous studies of SC noise in the spectral domain have shown that even in the long-pulse incoherent regime, ANDi SC exhibit superior shot-to-shot stability compared to conventional, anomalous dispersion SC [44]. While ANDi SC spectra fluctuate in close correlation around a long-term mean, conventional SC exhibit more chaotic, radical fluctuations in which a single-shot spectrum does not resemble at all the long-term mean. Here we observe the same effect in the time domain. The compressed ANDi SC pulses in Fig. 1 (c) are surprisingly robust against quantum and technical noise and fluctuate closely around their long-term mean, although the coherence function has completely collapsed. In contrast, previous studies of compressed conventional SC pulses describe the appearance of chaotic pulse shape variations

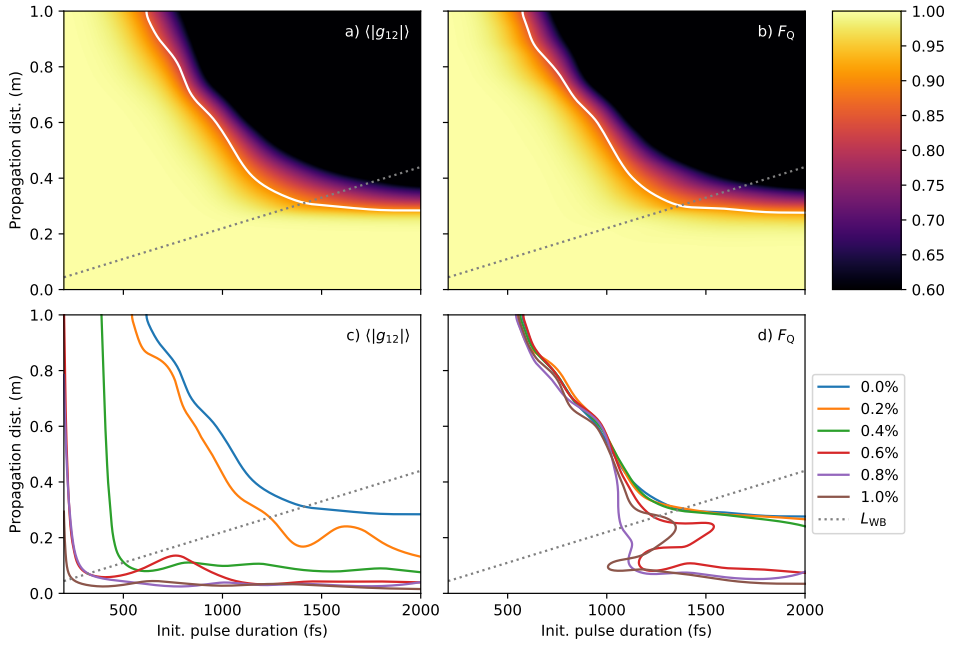

Fig. 2. Comparison between mean coherence $\langle|g_{12}|\rangle$ and quality factor F_Q as function of input pulse duration and propagation distance. Dashed lines show L_{WB}. (a) $\langle|g_{12}|\rangle$ and (b) F_Q heat map considering shot noise only (no technical noise). Solid lines show L_C and L_Q, respectively. (c) L_C and (d) L_Q for various levels of programmed input RIN δ_I.

from shot-to-shot as soon as the coherence function starts to decrease, severely degrading the quality of the mean compressed pulse [8, 9]. These statistical properties of ANDi SC imply that averaging over a relatively small ensemble size of 20 independent simulations is sufficient to extract the noise characteristics of the mean field, as confirmed by [35], while the ensemble size would have to be much larger for conventional SC [44].

4.1. Correlation of coherence and compressed pulse quality

In Fig. 2 we investigate the correlation of average coherence $\langle|g_{12}|\rangle$ and compressed pulse quality F_Q in the presence of quantum and technical noise in more detail. $\langle|g_{12}|\rangle$ is plotted in Fig. 2 (a) as function of pump pulse duration and propagation distance for a fixed input peak power of $P_0 = 100$ kW, taking into account only the quantum noise term δ_N, i.e. in the absence of technical noise ($\delta_A = 0$). The optical wave-breaking length L_{WB} is indicated as a dashed line, marking the typical length scale required for the SC to develop its full spectral bandwidth [1, 45]. The solid contour line shows where $\langle|g_{12}|\rangle = 0.9$, defining the coherence length L_C and the border between coherent and incoherent spectral broadening. This figure essentially reproduces the results discussed in detail in Ref. [28]. Highly coherent, fully developed, near-octave spanning SC can be generated where $L_{WB} < L_C$, i.e. up to $T_{0,FWHM} \sim 1.4$ ps. In the yellow, highly coherent regions self-phase modulation (SPM) and optical wave breaking (OWB) dominate the nonlinear dynamics, while in the black region the interplay of SRS and FWM leads to decoherence in the form of incoherent cloud formation and incoherent optical wave-breaking [28].

In Fig. 2 (b) we repeat the calculations in (a), but using the pulse quality factor F_Q. L_{WB} is again indicated by the dashed line, and the solid contour line marks $F_Q = 0.9$, defining the

length scale $L_Q = \max(z|_{F_Q \geq 0.9})$ as the maximum propagation distance allowing high-quality pulse compression. If $L_{WB} < L_Q$, high quality, single-cycle pulses can be generated. Since Figs. 2 (a) and (b) are virtually identical, we conclude that in the absence of technical noise $\langle|g_{12}|\rangle$ and F_Q are highly correlated over the entire investigated parameter space. Therefore, under these circumstances the coherence parameters $\langle|g_{12}|\rangle$ and $L_C \simeq L_Q$ are good figures of merit describing accurately the pulse quality that can be expected in an ultrafast nonlinear compression experiment. This result confirms previous reports of a strong correlation between coherence and compressed pulse quality obtained for conventional, anomalous-dispersion SC [9], and extends this observation to the case of ANDi SC.

However, the situation changes when technical noise is considered. Figs. 2 (c) and (d) show how L_C and L_Q, i.e. the 0.9 contour lines in Figs. 2 (a) and (b), respectively, react to varying amount of technical noise. L_C collapses dramatically even for small amounts of technical noise, since $\langle|g_{12}|\rangle$ reacts sensitively to low-frequency technical fluctuations as was shown in Fig. 1. The range of pump pulse durations that fulfil the condition $L_{WB} < L_C$ for the generation of fully developed, highly coherent SC reduces to ≤ 400 fs for 0.4% RIN and even ≤ 100 fs for 0.9% RIN. This qualitatively confirms the results reported recently by Genier et al. [35]. However, in stark contrast to this strong reaction of the coherence, L_Q and consequently also F_Q are barely affected by technical noise for input pulse durations ≤ 1 ps. In our simulations we observe significantly degrading compressed pulse quality only in the range where decoherence due to quantum noise amplification by SRS and FWM occurs, i.e. in the parameter space defined by the black regions of Figs. 2 (a) and (b). Hence, the strong correlation of coherence and pulse quality is violated in the presence of technical noise. The additional coherence collapse of Fig. 2 (c) caused by low-frequency technical noise does not correspond to a significant degradation of pulse quality in an ultrafast experiment, and in fact has also very limited impact in the spectral domain, as shown in Fig. 1 and Ref. [35].

The comparison between pulse quality and coherence is extended in Fig. 3, which shows the evolution of both metrics as a 1 ps, 100 kW pump pulse propagates through the fiber considering (a) only quantum noise, and (b) additional 0.7% RIN. While the correlation is nearly perfect when only quantum noise is considered, it collapses in the presence of technical noise. In fact, the evolution of F_Q is virtually unaffected by the additional technical noise. We note that the small dips of F_Q in (b) and in Fig. 2 (d) at $z < L_{WB}$ are caused by slightly different rates of spectral broadening for different noise seeds. These differences are minimized when the SC is fully developed at $z > L_{WB}$. It is clear that the the amplification of quantum noise by incoherent nonlinear dynamics has a much larger impact on ultrafast experiments than technical noise, and the limits of coherence calculated with the quantum noise term only and outlined in Ref. [28] are useful for the description of the temporal stability of the SC pulses, even if the laser exhibits a reasonable amount ($\leq 1\%$) of RIN.

Figs. 3 (c) and (d) show the mean coherence and quality factor, respectively, at $z = 1.5L_{WB}$ as we increase technical noise for various inital pulse durations. We consider $z = 1.5L_{WB}$ as this is a reasonable fiber length to ensure that the SC is fully developed while avoiding excessive quantum noise amplification [28]. For a 200 fs pulse, $1.5L_{WB}$ corresponds to 6.6 cm and at this distance even the strongest technical noise considered here does not affect the coherence significantly. While $\langle|g_{12}|\rangle$ drops substantially with increasing pump pulse duration and technical noise level, in agreement with the findings of Genier et al. [35], F_Q does not drop below 0.9 in all cases for $T_{0,FWHM} \leq 1$ ps. Only when incoherent broadening dynamics dominate, i.e. for $T_{0,FWHM} > 1.4$ ps, both $\langle|g_{12}|\rangle$ and F_Q remain low, independent of the technical noise level.

4.2. Noise amplification

In contrast to previous studies focusing on the ANDi SC noise in the spectral domain, our approach allows us to compare the noise characteristics of the pump pulses and the compressed

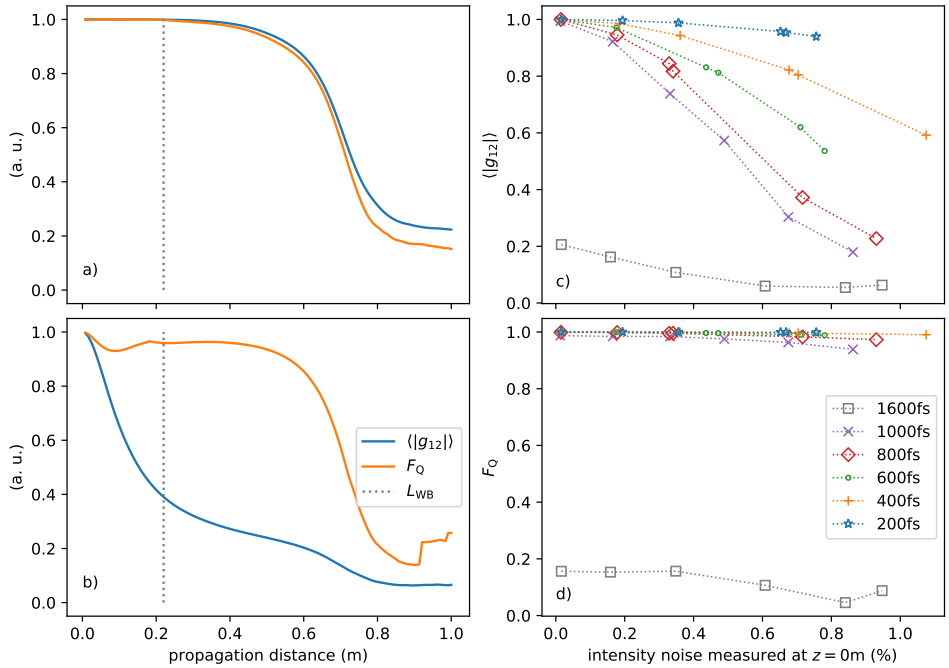

Fig. 3. Comparison of coherence and quality factor. On the left, evolution of those two metrics for a 1 ps pulse (a) considering shot noise only, and (b) with 0.7% input RIN. On the right, relationship between RIN measured at the fiber input and (c) coherence, (d) quality factor measured at $1.5L_{\mathrm{WB}}$ for various initial pulse durations.

pulses directly in the time domain. In this way we can easily determine whether the different types of technical noise experience suppression, amplification, or remain constant during the ANDi SC generation process. Fig. 4 shows the amplification factor for intensity and FWHM noise, defined as the ratio of the respective relative noise level of the compressed SC pulses at $z = 1.5L_{\mathrm{WB}}$ and the input pulses, for various pump pulse durations and input noise levels. In addition, we show the timing jitter of the compressed SC pulses in absolute values (femtoseconds) since we assume a perfectly periodic pulse train at the fiber input.

Our simulations validate in quantitative terms the very limited impact of technical noise on the ANDi SC generation dynamics. For $T_{0,\mathrm{FWHM}} \leq 800$ fs,the noise amplification factors show very little dependence on the technical noise level of the pump pulses. For these pump pulse durations we observe RIN and FWHM amplification factors in the range 1 - 3. For pump laser RIN < 0.3%, typical for many ultrafast mode-locked lasers, the noise of the SC is virtually identical to the pump laser. These results are confirmed by recent experimental measurements in the mid-IR spectral region, which found that the initial fluctuations of the pump laser are at most amplified by a factor of three, even for pump pulses of a few hundred femtoseconds duration and long fiber lengths [37].

Only for longer pump pulse durations we observe significant noise amplification, with the transition from stable to noisy SC generation occurring around $T_{0,\mathrm{FWHM}} \simeq 1000$ fs, where we observe an amplification of the input noise levels of approximately 10 dB. This coincides with the onset of quantum noise amplification due to incoherent SRS/FWM spectral broadening dynamics identified in Figs. 2 (a)-(b). It has to be noted, however, that the compressed pulse duration is still approx. 6 fs with quality factors $F_{\mathrm{Q}} > 0.9$, i.e. good quality sub-two cycle pulse generation with exceptional compression factor of ~ 160 is possible in this case. For comparison, we also

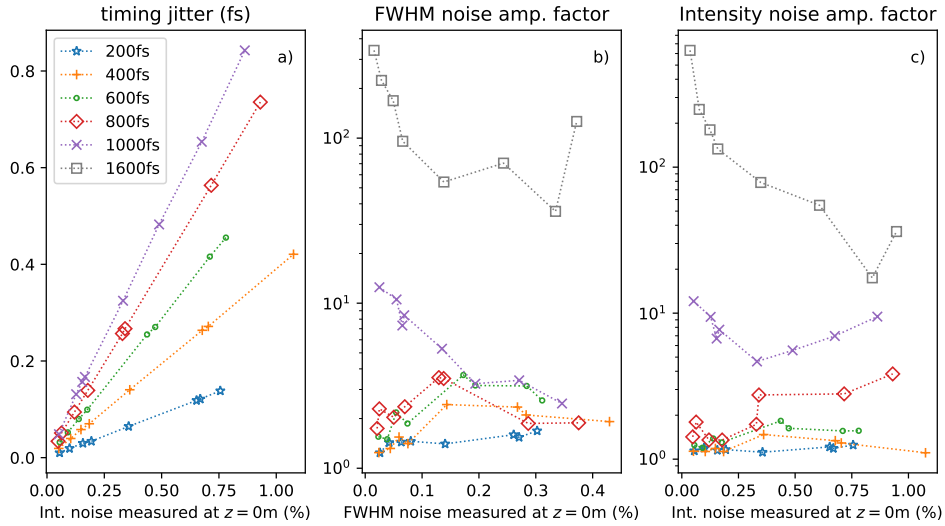

Fig. 4. Noise properties of the compressed pulses measured with a fiber length of $z = 1.5L_{\mathrm{WB}}$ as functions of initial pump pulse fluctuations: (a) standard deviation of timing jitter in fs as function of input RIN, (b) FWHM noise amplification factor as function of input FWHM noise, and (c) intensity noise amplification factor as function of the input RIN.

show the amplification factors for the $T_{0,\mathrm{FWHM}} = 1600$ fs pump pulse, for which $L_C < L_{\mathrm{WB}}$, i.e. decoherence due to incoherent SRS/FWM dynamics becomes significant before spectral broadening is concluded. Here we observe RIN amplification exceeding 20 dB for near shot-noise limited input. While this is substantial, it is significantly less than observed for conventional, anomalous dispersion SC, where nonlinear amplification factors for shot noise in the order of 90 dB were measured [26]. With our time domain analysis we can therefore confirm previous observations made in the spectral domain that even in the incoherent regime, ANDi SC exhibit better noise properties than the corresponding conventional SC [44]. The decrease of noise amplification with increasing technical noise level observed in the long-pulse regime can be understood by the fact that the absolute noise levels are dominated by amplified quantum noise and therefore remain approximately constant with increasing technical noise. Hence, the ratio of SC noise and input noise decreases with increasing input noise level.

We observe a linear increase of timing jitter with increasing technical noise level, with steeper slopes for longer pulse durations. For $T_{0,\mathrm{FWHM}} \leq 600$ fs the standard deviation of this jitter remains below 0.5 fs even for the highest considered technical noise levels, but reaches almost 0.9 fs in the long-pulse regime, i.e. almost 20% of the compressed pulse duration. Hence, in agreement with the observations in Fig. 1 timing jitter can be considered the dominating impact of technical noise on ultrafast SC experiments. Nevertheless, for the typical pump pulse durations and technical noise levels used in ultrafast experiments (< 400 fs, <0.5% RIN) the timing jitter introduced by the ANDi SC generation and compression process will hardly have practical consequences. It should be noted that commercial, unstabilized femtosecond laser cavities, which have been used as pump sources in most ultrafast ANDI SC applications to date, exhibit up to an order of magnitude larger timing jitters than those we have discussed here.

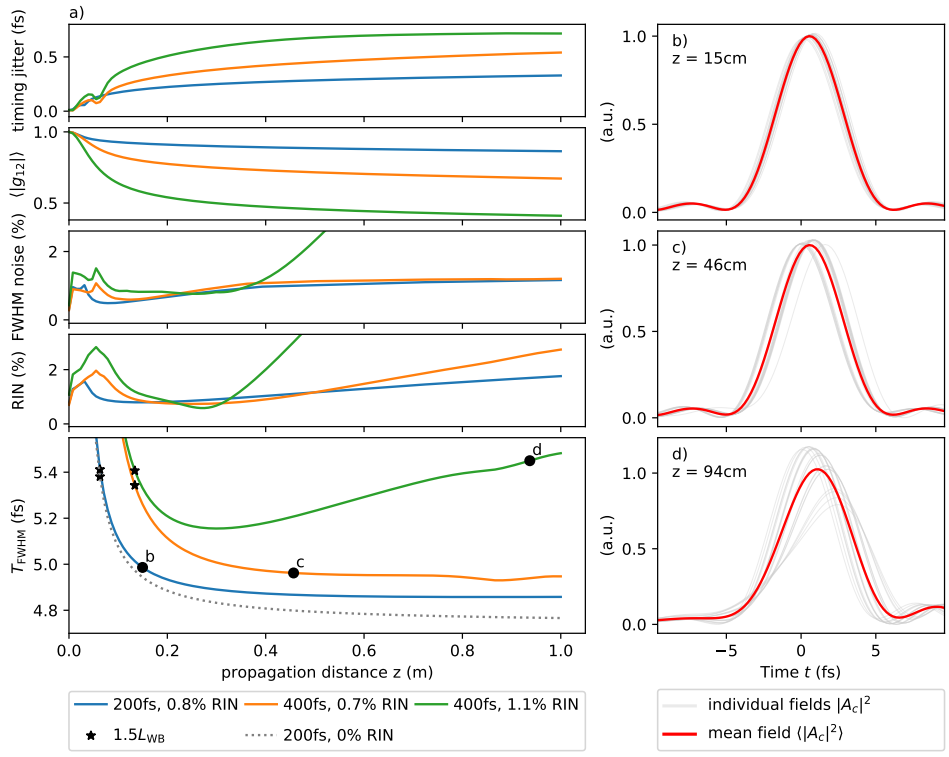

Fig. 5. (a) Evolution of timing jitter, mean coherence, FWHM noise, RIN and compressed mean pulse duration for three different sets of 100 kW pulses. Dashed line: theoretical limit computed by compressing a 200 fs pulse without technical noise assuming a flat phase. The legend indicates measured RIN at input. (b)-(d): illustrations of the mean and individual compressed pulses at three positions indicated in (a).

4.3. Noise evolution, obtainable pulse durations, and coherence - timing jitter correlation

Finally, we consider the actual duration of the mean compressed pulse as a function of the fiber length in Fig. 5 for three different sets of pump pulse durations and input noise levels. For each set we also study the evolution of timing jitter, mean coherence, FWHM noise, and RIN as functions of the fiber length. The resulting compressed pulse ensemble together with its mean multi-shot intensity is illustrated for three representative cases.

Despite a relatively large technical noise level with a RIN of 0.8%, the 200 fs input pulse can be compressed to 4.9 fs, corresponding to 1.4 optical cycles and a compression factor of 40, close to the theoretical limit computed by compressing a 200 fs pump pulse without technical noise to its Fourier limit. In agreement with previous experimental studies, we confirm the benefit of extending the fiber length beyond the wave-breaking length in order to reach the shortest compressed pulse durations [7]. For the 200 fs pulse, the compressed pulse duration drops continuously with increasing fiber length, which can be mainly attributed to spectral flattening occurring for longer propagation distances [28]. Of course, in a real experiment a longer fiber implies a larger amount of dispersion that has to be compensated, such that the effective fiber length is limited by the maximum phase shift available from a given compression device. RIN and FWHM noise remain below 1%, i.e. on the same level as the input, for $z < 0.4$ m and only rise slowly to 1.8% and 1.2%, respectively, for $z = 1$ m. The compressed pulse generally has a

very good quality, $F_Q = 1$, as illustrated in Fig. 5 (b).

The minimum obtainable pulse duration increases with longer pump pulses and higher input noise level. This effect is caused by an increasing amount of timing jitter (compare also Fig. 4 (a)) limiting the temporal duration of the mean intensity $\langle |A_c(t)|^2 \rangle$ measured in a multi-shot experiment. Nevertheless, the 400 fs, 0.7% RIN input pulse can be compressed to a high quality, sub-5 fs pulse with RIN and FWHM noise level of about 1%, as shown in Fig. 5 (c). Since L_{WB} is proportional to T_0, longer input pulses also require longer fiber lengths in order to reach the shortest possible compressed pulse durations.

For long pulses with input RIN levels exceeding approximately 1% we observe a qualitative change of the noise evolution along the fiber, which is exemplified by the 400 fs, 1.1% RIN input pulse (0.4% FWHM noise). The noise of the compressed pulse train reaches a minimum at a particular fiber length, $z = 0.27$ m in this case, where RIN is suppressed to 0.6%, i.e. nearly half of the input level, while FWHM noise doubles to 0.8%. This effect can be qualitatively understood by revisiting Fig. 1 (b) and noting that the main consequence of technical noise is a slight SC spectral bandwidth variation, which translates into FWHM noise of the compressed pulse train. The noise minimum also corresponds to the fiber length providing the minimum obtainable pulse duration (5.2 fs). For longer fibers, the noise of the compressed pulses increases almost linearly to reach levels exceeding 10% at $z = 1$ m. In this regime, the shot-to-shot fluctuations are substantial, as illustrated in Fig. 5 (d), causing an increase of the mean pulse duration. Nevertheless, the mean pulse is still of very good quality ($F_Q \sim 0.97$) that will be acceptable in many multi-shot ultrafast experiments, such as nonlinear imaging.

Interestingly, although the 400 fs, 1.1% RIN and the 400 fs, 0.7% RIN pump pulses show very different noise evolutions in Fig. 5 (b), their spectral evolution is virtually identical. Both show first signatures of incoherent SRS/FWM dynamics starting at about $z = 0.35$ m, which coincides with the onset of strong noise amplification for the 1.1% input noise level. Hence, it is conceivable that the effect of incoherent nonlinear dynamics is enhanced in the presence of high technical noise levels exceeding ~ 1% at the fiber input. While we could reproduce this effect in our simulations with different noise seeds, an input RIN > 1% falls outside of the systematically investigated parameter regime of this study. Therefore, our results provide an indication, but not conclusive evidence of such an interaction between technical and shot noise amplification.

Fig. 5 (a) also provides an explanation for the coherence collapse in the presence of technical noise discussed in Sec. 4.1 and by Genier et al. [35]. The drop of $\langle |g_{12}| \rangle$ is strongly correlated to the timing jitter introduced by technical fluctuations. This is easy to understand since the mutual coherence is a function of the relative time delay $t_1 - t_2$ between the SC spectra under consideration, i.e. $\langle |g_{12}| \rangle = \langle |g_{12}(\omega, t_1 - t_2)| \rangle$ in Eq. (7). Usually, $t_1 - t_2 = 0$ is assumed when SC coherence properties are discussed. For $t_1 - t_2 \neq 0$, i.e. when timing jitter is introduced, the value of $\langle |g_{12}| \rangle$ naturally drops due to the reduced temporal overlap between the pulses. Unlike in the shot-noise limited case, Figs. 2 - 5 clearly illustrate that in the presence of technical noise a reduced value of $\langle |g_{12}| \rangle$ is not a useful indication of excessive nonlinear noise amplification, reduced temporal pulse quality, or decoherence due to incoherent nonlinear dynamics, but merely reflects a non-zero timing jitter.

5. Conclusions

We have presented a detailed numerical study on the impact of technical pump laser fluctuations on octave-spanning ANDi SC generation and its application in ultrafast photonics. By simulating a realistic nonlinear pulse compression experiment, the noise characteristics of the input pulses and the compressed sub-two cycle pulses can be compared directly in the time domain. For pump pulse durations of less than 600 fs, input RIN <1%, and correctly chosen fiber lengths, we determine that the initial fluctuations of the pump laser are at most amplified by a factor of three. For the typically shorter pump pulse durations and lower technical noise levels used in ultrafast

experiments, the noise of the compressed pulse train is virtually identical to the pump laser noise. Longer pump pulses and higher input noise levels will require a more careful analysis in order to determine whether or not the resulting SC noise is acceptable for a particular application, and our results provide an important guideline in this regard. The amplification of shot noise by incoherent nonlinear dynamics assumes an increasingly dominating role for longer pump pulse durations and excessive fiber lengths, leading to noise amplification factors in the order of 10 for a 1 ps pump pulse and reaching 20 - 30 dB in the completely incoherent regime > 1.5 ps pump pulse duration. These results support the prevailing understanding that noise amplification by SC generation dynamics in the normal dispersion regime is substantially reduced in comparison to conventional, anomalous dispersion SC, where amplification factors of 20 dB for technical noise and up to 90 dB for shot noise were measured [25, 26].

Current conventional and commercial SC sources have been demonstrated to match or even surpass the brightness of synchrotrons from the visible up to 10.6 µm wavelength, which makes them ideal candidates for spectroscopy and high-resolution imaging applications [46]. However, the SC suffer from considerable RIN of 50% and more due to the stochastic nature of modulational instability which all current commercial SC sources are based on. Our results suggest that high brightness, low-noise SC sources with RIN < 5% can be realized by pumping silica ANDi fibers with long, high peak power pump pulses up to 1 ps duration, leading to average powers in the order of 10 W, e.g. for a 100 kW, 1 ps, 100 MHz pump source. Similarly, mid-IR ANDi SC sources have been demonstrated up to 12 µm wavelength, with brightness limited mainly by the low repetition rates of the employed pump sources [23]. Hence, the scaling of ANDi SC sources to the brightness levels of their commercial counterparts is mainly a question of developing suitable high repetition rate, low-noise pump sources.

We have shown that the previously reported drastic reduction of the ANDi SC coherence in the presence of technical noise is due to a timing jitter induced by technical fluctuations. While usually zero timing jitter is assumed in the calculation of the SC coherence function, pump laser fluctuations are translated to linear phase variations, which reduce the temporal overlap between the SC pulses under consideration. Our results demonstrate that the usual strong correlation between coherence and quality of the compressed pulses collapses in the presence of technical noise, and that in this situation $\langle |g_{12}| \rangle$ is not a useful figure of merit to judge pulse quality, noise amplification, or decoherence due to incoherent nonlinear dynamics. Except for the most demanding applications in precision metrology or attoscience, the minimal timing jitter and associated coherence degradation introduced by technical fluctuations will have no practical consequence for most ultrafast photonics applications currently employing ANDi SC sources. The amplification of shot noise by incoherent nonlinear dynamics has a much larger impact than technical noise on the quality and noise characteristics of the resulting ultrashort SC pulse train. Therefore, the limits of coherence determined with shot-noise limited input outlined in Ref. [28] remain useful, even if the laser exhibits a reasonable amount ($\leq 1\%$) of RIN.

Data availability

The raw data for the significant figures in this paper is available online at https://dx.doi.org/10.7892/boris.144958.

Funding

Schweizerischer Nationalfonds zur Förderung der Wissenschaftlichen Forschung (PCEFP2_181222).

Acknowledgments

Calculations were performed on UBELIX (http://www.id.unibe.ch/hpc), the HPC cluster at the University of Bern. The program is written in Python 3.7 [47] and makes heavy use

of NumPy [48] for scientific computing, Matplotlib [49] for plotting and Ray [50] for distributed computing.

Disclosures

The authors declare no conflicts of interest.

References

1. A. Heidt, A. Hartung, and H. Bartelt, "Generation of ultrashort and coherent supercontinuum light pulses in all-normal dispersion fibers," in *The Supercontinuum Laser Source: The Ultimate White Light,* (Springer, 2016), pp. 247–280.
2. H. Tu, Y. Liu, D. Turchinovich, and S. A. Boppart, "Compression of fiber supercontinuum pulses to the Fourier-limit in a high-numerical-aperture focus," Opt. Lett. **36**, 2315–2317 (2011).
3. A. M. Heidt, "Pulse preserving flat-top supercontinuum generation in all-normal dispersion photonic crystal fibers," J. Opt. Soc. Am. B **27**, 550–559 (2010).
4. L. E. Hooper, P. J. Mosley, A. C. Muir, W. J. Wadsworth, and J. C. Knight, "Coherent supercontinuum generation in photonic crystal fiber with all-normal group velocity dispersion," Opt. Express **19**, 4902–4907 (2011).
5. A. M. Heidt, J. Rothhardt, A. Hartung, H. Bartelt, E. G. Rohwer, J. Limpert, and A. Tünnermann, "High quality sub-two cycle pulses from compression of supercontinuum generated in all-normal dispersion photonic crystal fiber," Opt. Express **19**, 13873–13879 (2011).
6. S. Demmler, J. Rothhardt, A. M. Heidt, A. Hartung, E. G. Rohwer, H. Bartelt, J. Limpert, and A. Tünnermann, "Generation of high quality, 1.3 cycle pulses by active phase control of an octave spanning supercontinuum," Opt. Express **19**, 20151–20158 (2011).
7. Y. Liu, H. Tu, and S. A. Boppart, "Wave-breaking-extended fiber supercontinuum generation for high compression ratio transform-limited pulse compression," Opt. Lett. **37**, 2172–2174 (2012).
8. G. Chang, T. Norris, and H. Winful, "Optimization of supercontinuum generation in photonic crystal fibers for pulse compression," Opt. Lett. **28**, 546–8 (2003).
9. J. M. Dudley and S. Coen, "Fundamental limits to few-cycle pulse generation from compression of supercontinuum spectra generated in photonic crystal fiber," Opt. Express **12**, 2423–2428 (2004).
10. B. Schenkel, R. Paschotta, and U. Keller, "Pulse compression with supercontinuum generation in microstructure fibers," J. Opt. Soc. Am. B **22**, 687–693 (2005).
11. H. Tu and S. A. Boppart, "Coherent fiber supercontinuum for biophotonics," Laser Photonics Rev. **7**, 628–645 (2013).
12. H. Tu, Y. Liu, D. Turchinovich, M. Marjanovic, J. K. Lyngsø, J. Lægsgaard, E. J. Chaney, Y. Zhao, S. You, W. L. Wilson *et al.*, "Stain-free histopathology by programmable supercontinuum pulses," Nat. photonics **10**, 534 (2016).
13. A. M. Heidt, A. Hartung, G. W. Bosman, P. Krok, E. G. Rohwer, H. Schwoerer, and H. Bartelt, "Coherent octave spanning near-infrared and visible supercontinuum generation in all-normal dispersion photonic crystal fibers," Opt. Express **19**, 3775–3787 (2011).
14. J. Rothhardt, S. Hädrich, J. Delagnes, E. Cormier, and J. Limpert, "High average power near-infrared few-cycle lasers," Laser Photonics Rev. **11** (2017).
15. M. Krebs, S. Hädrich, S. Demmler, J. Rothhardt, A. Zaïr, L. Chipperfield, J. Limpert, and A. Tünnermann, "Towards isolated attosecond pulses at megahertz repetition rates," Nat. Photonics **7**, 555 (2013).
16. N. M. Kearns, A. C. Jones, M. B. Kunz, R. T. Allen, J. T. Flach, and M. T. Zanni, "Two-dimensional white-light spectroscopy using supercontinuum from an all-normal dispersion photonic crystal fiber pumped by a 70 MHz Yb fiber oscillator," J. Phys. Chem. A **123**, 3046–3055 (2019).
17. A. Rampur, Y. Stepanenko, G. Stępniewski, T. Kardaś, D. Dobrakowski, D.-M. Spangenberg, T. Feurer, A. Heidt, and M. Klimczak, "Ultra low-noise coherent supercontinuum amplification and compression below 100 fs in an all-fiber polarization-maintaining thulium fiber amplifier," Opt. Express **27**, 35041–35051 (2019).
18. K. Tarnowski, T. Martynkien, P. Mergo, J. Sotor, and G. Soboń, "Compact all-fiber source of coherent linearly polarized octave-spanning supercontinuum based on normal dispersion silica fiber," Sci. Rep. **9**, 12313 (2019).
19. A. M. Heidt, J. M. Hodasi, A. Rampur, D.-M. Spangenberg, M. Ryser, M. Klimczak, and T. Feurer, "Low noise all-fiber amplification of a coherent supercontinuum at 2μm and its limits imposed by polarization noise," arXiv preprint arXiv:1903.09583 (2019).
20. N. Nishizawa, "Wideband ultrafast fiber laser sources for OCT and metrology," J. Phys. B **49**, 182003 (2016).
21. K. P. Herdzik, K. N. Bourdakos, P. B. Johnson, A. P. Lister, A. P. Pitera, C.-y. Guo, P. Horak, D. J. Richardson, J. H. Price, and S. Mahajan, "Multimodal spectral focusing CARS and SFG microscopy with a tailored coherent continuum from a microstructured fiber," Appl. Phys. B **126**, 1–13 (2020).
22. M. Diouf, A. B. Salem, R. Cherif, H. Saghaei, and A. Wague, "Super-flat coherent supercontinuum source in As 38.8 Se 61.2 chalcogenide photonic crystal fiber with all-normal dispersion engineering at a very low input energy," Appl. Opt. **56**, 163–169 (2017).
23. N. Zhang, X. Peng, Y. Wang, S. Dai, Y. Yuan, J. Su, G. Li, P. Zhang, P. Yang, and X. Wang, "Ultrabroadband and coherent mid-infrared supercontinuum generation in Te-based chalcogenide tapered fiber with all-normal dispersion," Opt. Express **27**, 10311–10319 (2019).

24. J. Rothhardt, A. M. Heidt, S. Hädrich, S. Demmler, J. Limpert, and A. Tünnermann, "High stability soliton frequency-shifting mechanisms for laser synchronization applications," JOSA B **29**, 1257–1262 (2012).
25. N. R. Newbury, B. Washburn, K. L. Corwin, and R. Windeler, "Noise amplification during supercontinuum generation in microstructure fiber," Opt. Lett. **28**, 944–946 (2003).
26. K. L. Corwin, N. R. Newbury, J. M. Dudley, S. Coen, S. A. Diddams, K. Weber, and R. S. Windeler, "Fundamental noise limitations to supercontinuum generation in microstructure fiber," Phys. Rev. Lett. **90**, 113904 (2003).
27. J. Dudley, G. Genty, and S. Coen, "Supercontinuum generation is photonic crystal fiber," Rev. Mod. Phys. **78**, 1135–1184 (2006).
28. A. M. Heidt, J. S. Feehan, J. H. V. Price, and T. Feurer, "Limits of coherent supercontinuum generation in normal dispersion fibers," J. Opt. Soc. Am. B **34**, 764–775 (2017).
29. I. B. Gonzalo, R. D. Engelsholm, M. P. Sørensen, and O. Bang, "Polarization noise places severe constraints on coherence of all-normal dispersion femtosecond supercontinuum generation," Sci. Rep. **8**, 6579 (2018).
30. J. S. Feehan and J. H. Price, "Decoherence due to XPM-assisted Raman amplification for polarization or wavelength offset pulses in all-normal dispersion supercontinuum generation," J. Opt. Soc. Am. B **37**, 635–644 (2020).
31. Y. Liu, Y. Zhao, J. Lyngsø, S. You, W. L. Wilson, H. Tu, and S. A. Boppart, "Suppressing short-term polarization noise and related spectral decoherence in all-normal dispersion fiber supercontinuum generation," J. Light. Technol. **33**, 1814–1820 (2015).
32. G. Genty, S. Coen, and J. M. Dudley, "Fiber supercontinuum sources (invited)," J. Opt. Soc. Am. B **24**, 1771–1785 (2007).
33. U. Møller and O. Bang, "Intensity noise in normal-pumped picosecond supercontinuum generation, where higher-order Raman lines cross into anomalous dispersion regime," Electron. Lett. **49**, 63–65 (2013).
34. N. Nishizawa, T. Niinomi, Y. Nomura, L. Jin, and Y. Ozeki, "Octave spanning coherent supercontinuum comb generation based on Er-doped fiber lasers and their characterization," IEEE J. Sel. Top. Quantum Electron. **24**, 1–9 (2018).
35. E. Genier, P. Bowen, T. Sylvestre, J. M. Dudley, P. Moselund, and O. Bang, "Amplitude noise and coherence degradation of femtosecond supercontinuum generation in all-normal-dispersion fibers," J. Opt. Soc. Am. B **36**, A161–A167 (2019).
36. S. Rao D.S., R. D. Engelsholm, I. B. Gonzalo, B. Zhou, P. Bowen, P. M. Moselund, O. Bang, and M. Bache, "Ultra-low-noise supercontinuum generation with a flat near-zero normal dispersion fiber," Opt. Lett. **44**, 2216–2219 (2019).
37. Z. Eslami, P. Ryczkowski, L. Salmela, and G. Genty, "Low-noise octave-spanning mid-infrared supercontinuum generation in a multimode chalcogenide fiber," Opt. Lett. **45**, 3103–3106 (2020).
38. A. Rieznik, A. M. Heidt, P. Konig, V. A. Bettachini, and D. Grosz, "Optimum integration procedures for supercontinuum simulation," IEEE Photonics J. **4**, 552–560 (2012).
39. J. Hult, "A fourth-order Runge–Kutta in the interaction picture method for simulating supercontinuum generation in optical fibers," J. Light. Technol. **25**, 3770–3775 (2008).
40. A. M. Heidt, "Efficient adaptive step size method for the simulation of supercontinuum generation in optical fibers," J. Light. Technol. **27**, 3984–3991 (2009).
41. K. Saitoh and M. Koshiba, "Empirical relations for simple design of photonic crystal fibers," Opt. Express **13**, 267–274 (2005).
42. M. Koshiba and K. Saitoh, "Applicability of classical optical fiber theories to holey fibers," Opt. Lett. **29**, 1739–1741 (2004).
43. Q. Lin and G. P. Agrawal, "Raman response function for silica fibers," Opt. Lett. **31**, 3086–3088 (2006).
44. S. Dupont, Z. Qu, S.-S. Kiwanuka, L. E. Hooper, J. C. Knight, S. R. Keiding, and C. F. Kaminski, "Ultra-high repetition rate absorption spectroscopy with low noise supercontinuum radiation generated in an all-normal dispersion fibre," Laser Phys. Lett. **11**, 075601 (2014).
45. C. Finot, B. Kibler, L. Provost, and S. Wabnitz, "Beneficial impact of wave-breaking for coherent continuum formation in normally dispersive nonlinear fibers," J. Opt. Soc. Am. B **25**, 1938–1948 (2008).
46. C. R. Petersen, P. M. Moselund, L. Huot, L. Hooper, and O. Bang, "Towards a table-top synchrotron based on supercontinuum generation," Infrared Phys. Technol. **91**, 182–186 (2018).
47. G. Van Rossum and F. L. Drake, *Python 3 Reference Manual* (CreateSpace, Scotts Valley, CA, 2009).
48. T. Oliphant, "A guide to NumPy," USA: Trelgol Publishing (2006–).
49. J. D. Hunter, "Matplotlib: A 2d graphics environment," Comput. Sci. & Eng. **9**, 90–95 (2007).
50. P. Moritz, R. Nishihara, S. Wang, A. Tumanov, R. Liaw, E. Liang, M. Elibol, Z. Yang, W. Paul, M. I. Jordan, and I. Stoica, "Ray: A distributed framework for emerging AI applications," (2017).